Journal of Theoretical and Applied Mechanics, Sofia, Vol.48 No.4 (2018) pp. 61-77
SOLID MECHANICS

ANALYTICAL STUDY OF ELASTIC-PLASTIC FRACTURE IN THE CRACK-LAP SHEAR MULTILAYERED BEAM CONFIGURATION

VICTOR RIZOV*

Department of Technical Mechanics, University of Architecture, Civil Engineering and Geodesy, 1 Chr. Smirnensky blvd, Sofia, Bulgaria

[Received XXX. Accepted 08 October 2018]

ABSTRACT: This paper reports an analytical study of delamination fracture in the Crack-Lap Shear (CLS) multilayered beam configuration with taking into account the material non-linearity. A delamination crack was located arbitrary along the beam height. It was assumed that the CLS mechanical response can be described by using a power-law stress-strain relation. It should be mentioned that each layer may have different material constants in the stress-strain relation. Besides, the thickness of each layer may be different. The classical beam theory was applied in the present study. The non-linear fracture behaviour was analyzed by the J-integral. Analytical solutions of the J-integral were obtained for homogeneous as well as for multilayered CLS beams. In order to verify the solutions obtained, analyses of the strain energy release rate were developed with considering material non-linearity. Material properties and crack location effects on the non-linear fracture behaviour were investigated. The analysis revealed that the J-integral value increases when the material non-linearity is taken into account. It was found also that the J-integral value decreases with increasing the lower crack arm thickness. The approach developed here is very convenient for parametric fracture analyses. The solutions derived can be used for optimization of the CLS multilayered beams with respect to their fracture performance.

KEY WORDS: fracture, multilayered beam, material non-linearity, J-integral, analytical modelling.

1 INTRODUCTION

Multilayered materials have many useful properties, such as high strength-to-weight and high stiffness-to-weight ratios which facilitate their extensive use in structural components. Also, multilayered materials are becoming more common in applications where barrier properties are an issue. The growing interest in structural applications has been followed by increasing demand to ensure their safe operations. One of

*Corresponding author e-mail: v_rizov_fhe@uacg.bg

the main concerns is their high susceptibility to delamination fracture. Although a delamination crack between layers usually has little or no visible signs of such from the outside, it can drastically reduce the strength, durability and stability of the layered structure. This fact clearly indicates the need of studying the delamination fracture in layered materials. For the recent decades, the delamination fracture behaviour has been extensively investigated [1–8] mainly by using various beam specimens.

Linear-elastic fracture behaviour of multilayered beam specimens was studied in [9]. The analysis was carried-out in terms of the total strain energy release rate. For this purpose, a general multilayered beam model was used. The crack arms and the intact beam portion (ahead of the crack tip) were analyzed as equivalent homogeneous linear-elastic beams. The strain energy release rate associated with the crack growth was obtained in a function of the bending moments and axial forces in the cross-sections behind and ahead of the crack tip. The method developed was applied to study the delamination fracture in several multilayered beam configurations.

Delamination fracture behaviour of multilayered beams subjected to four-point bending was analyzed by using methods of linear-elastic fracture mechanics [10]. For this purpose, the classical beam theory was applied (the crack arms and the uncracked beam portion were modelled as linear-elastic beams). The general closed form analytical solution was derived for the total strain energy release rate in a function of the bending moment. The solution is valid for multilayered beam configurations with any number of layers (each layer may have different thickness and modulus of elasticity). Besides, the fracture can occur at any interface.

The total strain energy release rate in a four-layer linear-elastic beam was analyzed in [11]. A delamination crack is located between the second and the third layers. By applying the classical beam theory, an analytical expression for the strain energy release rate was derived in a function of the elasticity modulus, thickness of the layers and the crack tip cross-sectional bending moment. The effect of thickness ratio between the adjacent layers was discussed.

While many researchers have studied the delamination fracture in multilayered beams assuming validity of the Hooke's law, the purpose of present paper is to develop a fracture analysis of the CLS multilayered beam configuration with considering the material non-linearity.

2 Non-Linear Fracture Study of the CLS Beam

The multilayered CLS beam under investigation is reported schematically in Fig. 1. The number of layers is arbitrary. Besides, layers have different thickness. A perfect adhesion is assumed between layers. A vertical notch is cut in the beam mid-span in order to generate conditions for delamination cracking. There is a delamination crack of length $2a$ located symmetrically with respect to the beam mid-span. The

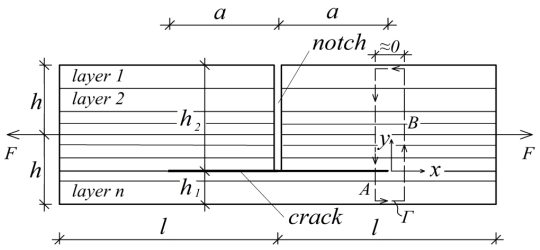

Fig. 1. The geometry and loading of CLS multilayered beam configuration.

thickness of lower crack arm is h_1. The upper crack arm is stress free. The beam has a rectangular cross-section of width, b, and height, $2h$. The loading consists of two longitudinal forces, F, applied centrically at the beam free ends as shown in Fig. 1.

The non-linear fracture behaviour of CLS configuration was studied theoretically by using the J-integral approach [12–14]. The J-integral was written as

$$J = \int_{\Gamma} \left[u_0 \cos\alpha - \left(p_x \frac{\partial u}{\partial x} + p_y \frac{\partial v}{\partial x} \right) \right] ds, \tag{1}$$

where Γ is a contour of integration going from the lower crack face to the upper crack face in the counter clockwise direction, u_0 is the strain energy density, α is the angle between the outwards normal vector to the contour of integration and the crack direction, p_x and p_y are the components of stress vector, u and v are the components of displacement vector with respect to the crack tip coordinate system xy, and ds is a differential element along the contour Γ.

The non-linear mechanical response of CLS beam layers was described by using power-law stress-strain curves that are symmetric for tension and compression (Fig. 2)

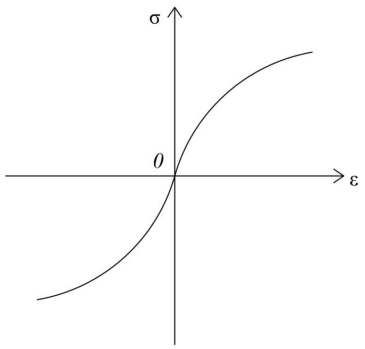

Fig. 2. Stress-strain curve.

$$\sigma_i = H_{1i}\varepsilon_i^{n_{1i}}, \quad i = 1, 2, , \ldots, n, \tag{2}$$

where σ_i and ε_i are the stresses and strains distributions in the i-th layer of multi-layered beam, H_{1i} and n_{1i} are material constants in the i-th layer, n is the layers number.

2.1 Investigation of homogeneous CLS beam

An investigation was carried-out first assuming that the CLS beam is homogeneous (Fig. 3). Therefore, the stress-strain relation was written as

$$\sigma = H_1\varepsilon^{n_1}, \tag{3}$$

where σ and ε are the stresses and strains, H_1 and n_1 are material constants.

Only half of the beam was considered in the fracture analysis due to the symmetry. The J-integral was solved by using an integration contour, Γ, that consists of the beam cross-sections behind and ahead of the crack tip (Fig. 3). It is obvious that the J-integral value is other non-zero only in segments A and B of the integration contour (Fig. 3). Therefore, the J-integral solution was obtained by summation

$$J = J_A + J_B, \tag{4}$$

where J_A and J_B are the J-integral values in the integration contour segments A and B, respectively.

The segment, A, coincides with the lower crack arm cross-section (Fig. 3). The lower crack arm is loaded non-centrically by a tensile force, F. Thus, the axial load, N, and the bending moment, M, in the lower crack arm were written as

$$N = F, \tag{5}$$

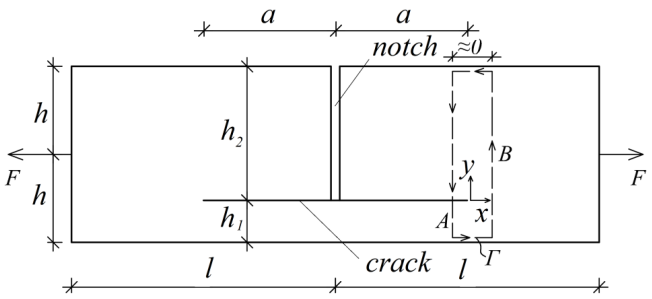

Fig. 3. The CLS homogeneous beam.

$$M = -F\left(h - \frac{h_1}{2}\right). \tag{6}$$

The components of J-integral in the lower crack arm were written as

$$p_x = -\sigma = -H_1\varepsilon^{n_1}, \tag{7}$$

$$p_y = 0. \tag{8}$$

According to the Bernoulli's hypothesis for plane sections, the strain, ε, in eq. (7) is distributed linearly along the cross-section height. Thus,

$$\varepsilon = \kappa_1 \left(z_1 - z_{1n_1}\right), \tag{9}$$

where κ_1 is the lower crack arm curvature, z_{1n_1} is the coordinate of the neutral axis (the neutral axis, $n_1 - n_1$, shifts from the centroid, since $N \neq 0$ (Fig. 4)). It should be noted that the Bernoulli's hypothesis for plane sections has been widely applied when analyzing delamination fracture in multilayered beams [10, 11]. Besides, the Bernoulli's hypothesis is used since beams of large span to height ratio loaded in eccentric tension are under consideration in the present paper.

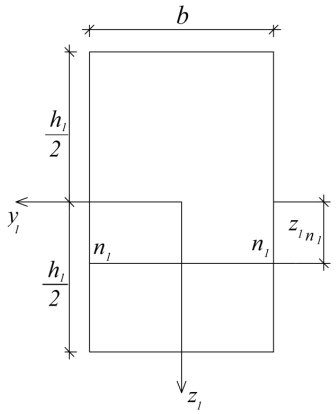

Fig. 4. Cross-section of the lower crack arm of CLS homogeneous beam.

We considered the elementary forces equilibrium in the cross-section in order to determine κ_1 and z_{1n_1}

$$N = \int_{-h_1/2}^{h_1/2} \sigma b dz_1, \tag{10}$$

$$M = \int_{-h_1/2}^{h_1/2} \sigma b z_1 dz_1. \tag{11}$$

By substituting of (3) and (9) in (10) and (11) and solving the integrals, we obtained

$$N = \frac{H_1 b \kappa_1^{n_1}}{n_1+1}\left[\left(\frac{h_1}{2}-z_{1n_1}\right)^{n_1+1}-\left(-\frac{h_1}{2}-z_{1n_1}\right)^{n_1+1}\right], \tag{12}$$

$$M = H_1 b \kappa_1^{n_1}\left[\frac{\left(\frac{h_1}{2}-z_{1n_1}\right)^{n_1+2}}{n_1+2}+\frac{\left(\frac{h_1}{2}-z_{1n_1}\right)^{n_1+1}z_{1n_1}}{n_1+1}\right. \\ \left.-\frac{\left(-\frac{h_1}{2}-z_{1n_1}\right)^{n_1+2}}{n_1+2}-\frac{\left(-\frac{h_1}{2}-z_{1n_1}\right)^{n_1+1}z_{1n_1}}{n_1+1}\right]. \tag{13}$$

From (12) and (13), we obtained

$$\kappa_1^{n_1} = \frac{N(n_1+1)}{H_1 b\left[\left(\frac{h_1}{2}-z_{1n_1}\right)^{n_1+1}-\left(-\frac{h_1}{2}-z_{1n_1}\right)^{n_1+1}\right]}, \tag{14}$$

$$\frac{N}{M}\left\{\left[\frac{n_1+1}{n_2+2}\frac{\left(\frac{h_1}{2}-z_{1n_1}\right)^{n_1+2}-\left(-\frac{h_1}{2}-z_{1n_1}\right)^{n_1+2}}{\left(\frac{h_1}{2}-z_{1n_1}\right)^{n_1+1}-\left(-\frac{h_1}{2}-z_{1n_1}\right)^{n_1+1}}\right]+z_{1n_1}\right\}-1=0, \tag{15}$$

where N and M are determined by (5) and (6), respectively.

It is obvious that at $n_1 = 1$ and $H_1 = E$ (here E is the modulus of elasticity) equation (3) transforms into the Hooke's law. This means that at $n_1 = 1$ and $H_1 = E$, equations (14) and (15) have to transform in the equations of curvature and coordinate of neutral axis of a linear-elastic beam. Indeed, at $n_1 = 1$ and $H_1 = E$ from (14) and (15), we obtained

$$\kappa_1 = \frac{12M}{Ebh_1^3}, \tag{16}$$

$$z_{1n_1} = -\frac{N}{M}\frac{h_1^2}{12}, \tag{17}$$

which are the curvature of lower crack arm and the coordinate of neutral axis at linear-elastic behaviour of the beam.

Equation (15) should be solved with respect to z_{1n_1} by using the MatLab program system at $n_1 \neq 1$. The result obtained should be substituted in (14) in order to determine the curvature.

For the other components of J-integral in the lower crack arm cross-section (Fig. 3 and Fig. 4), we have $ds = dz_1$ and $\cos\alpha = -1$.

The following formula from mechanics of materials was used to obtain the partial derivative that participates in (1):

$$\frac{\partial u}{\partial x} = \varepsilon \,. \tag{18}$$

In view of (9), formula (18) was written as

$$\frac{\partial u}{\partial x} = \kappa_1 \left(z_1 - z_{1n_1}\right), \tag{19}$$

where κ_1 and z_{1n_1} are determined from (14) and (15).

The strain energy density, u_0, is equal to the area OPQ enclosed by the stress-strain curve [15–18] (refer to Fig. 5)

$$u_0 = \int_0^{\varepsilon} H_1 \varepsilon^{n_1} d\varepsilon \,. \tag{20}$$

By solving the integral (20), we obtained

$$u_0 = H_1 \frac{\varepsilon^{n_1+1}}{n_1+1} \,. \tag{21}$$

In view of (9), formula (21) was written as

$$u_0 = H_1 \frac{\left[k_1 \left(z_1 - z_{1n_1}\right)\right]^{n_1+1}}{n_1+1} \,. \tag{22}$$

We substituted (7), (8), (9), (19) and (22) in (1). The solution of (1) was found as

$$J_A = \frac{H_1 n_1 \kappa_1^{n_1+1}}{(n_1+1)(n_1+2)} \left[\left(\frac{h_1}{2} - z_{1n_1}\right)^{n_1+2} - \left(-\frac{h_1}{2} - z_{1n_1}\right)^{n_1+2}\right]. \tag{23}$$

The segment, B, of integration contour coincides with the cross-section of un-cracked beam portion ahead of the crack tip (Fig. 3). The components of J-integral in segment B of the integration contour (Fig. 3) were written as $ds = -dz_3$ and $\cos\alpha = 1$, where z_3 varies in the interval $[-h;\ h]$. The un-cracked beam portion of CLS is loaded in centric tension (Fig. 3). Therefore, the other components of J-integral in segment B were determined as

$$p_x = \sigma = \frac{F}{2bh} \,, \qquad p_y = 0 \,. \tag{24}$$

By combining of (3) and (24), the partial derivative was obtained as

$$\frac{\partial u}{\partial x} = \varepsilon = \left(\frac{\sigma}{H_1}\right)^{1/n_1} = \left(\frac{F}{2bhH_1}\right)^{1/n_1} . \tag{25}$$

The strain energy density, u_0, was found by substituting of (25) in (21)

$$u_0 = \frac{H_1}{n_1+1}\Big(\frac{F}{2bhH_1}\Big)^{(n_1+1)/n_1}. \tag{26}$$

The J-integral solution in segment B of the integration contour (Fig. 3) was found by substituting of (24), (25) and (26) in (1)

$$J_B = 2h\frac{H_1}{n_1+1}\Big(\frac{F}{2bhH_1}\Big)^{(n_1+1)/n_1} - \frac{F}{b}\Big(\frac{F}{2bhH_1}\Big)^{1/n_1}. \tag{27}$$

Finally, (23) and (27) were substituted in (4) and the expression derived was doubled in view of the symmetry

$$J = \frac{2H_1 n_1 \kappa_1^{n_1+1}}{(n_1+1)(n_1+2)}\Big[\Big(\frac{h_1}{2}-z_{1n_1}\Big)^{n_1+2} - \Big(-\frac{h_1}{2}-z_{1n_1}\Big)^{n_1+2}\Big] + 4h\frac{H_1}{n_1+1}\Big(\frac{F}{2bhH_1}\Big)^{\frac{n_1+1}{n_1}} - \frac{2F}{b}\Big(\frac{F}{2bhH_1}\Big)^{1/n_1}. \tag{28}$$

It should be noted that at $n_1 = 1$, $H_1 = E$ and $h_1 = h$ equation (28) transforms in

$$J = \frac{7F^2}{2Eb^2h}, \tag{29}$$

which coincides with the formula for strain energy release rate when the crack is located in the mid-plane of homogeneous linear-elastic CLS beam [19].

In order to verify the non-linear solution (28), an analysis was developed of the strain energy release rate, G, in the CLS beam configuration with taking into account the non-linear material behaviour. For this purpose, an elementary increase of the crack area, dA_a, was assumed leading to the following expression of strain energy release rate:

$$G = \frac{dW_{ext} - dU}{dA_a}, \tag{30}$$

where dW_{ext} and dU are the changes of external work and strain energy, respectively. The change of external work was written as

$$dW_{\text{ext}} = dU^* + dU, \tag{31}$$

where dU^* is the change of complimentary strain energy. By substitution of (31) in (30), we derived

$$G = \frac{dU^*}{dA_a}, \tag{32}$$

where

$$dA_a = bda\,. \tag{33}$$

Here, da is an elementary crack length increase.

In order to determine the complimentary strain energy, U^*, the complimentary strain energy density, u_0^*, was integrated in the beam volume

$$U^* = \int_{-\frac{h_1}{2}}^{h_1/2} u_0^* bad z_1 + \int_{-h}^{h} u_0^* b(l-a) dz_3\,. \tag{34}$$

The complimentary strain energy density, u_0^*, is equal to area *OQR* that supplements area *OPQ* to a rectangle (Fig. 5). Therefore, the complimentary strain energy density was written as

$$u_0^* = \sigma\varepsilon - u_0\,. \tag{35}$$

By substitution of (3) and (21) in (35), we obtained

$$u_0^* = H_1 \frac{n_1 \varepsilon^{n_1+1}}{n_1+1}\,. \tag{36}$$

It should be specified that the strain, ε, in (36) is calculated by (9) in the lower crack arm. In the un-cracked beam portion, the strain, ε, that participates in (36) is obtained by (25).

After substitution of (9), (25) and (36) in (34), we derived

$$\begin{aligned} U^* = {} & \frac{abH_1 n_1 \kappa_1^{n_1+1}}{(n_1+1)(n_1+2)} \Big[\Big(\frac{h_1}{2} - z_{1n_1} \Big)^{n_1+2} - \Big(-\frac{h_1}{2} - z_{1n_1} \Big)^{n_1+2} \Big] \\ & + b(l-a) \Big[-4h \frac{H_1}{n_1+1} \Big(\frac{F}{2bhH_1} \Big)^{(n_1+1)/n_1} + \frac{2F}{b} \Big(\frac{F}{2bhH_1} \Big)^{1/n_1} \Big]. \end{aligned} \tag{37}$$

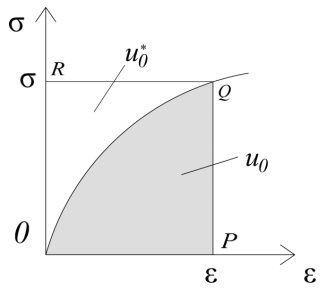

Fig. 5. Strain energy density u_0 and complimentary strain energy density u_0^*.

The expression obtained by combining of (32), (33) and (37) was doubled, since there are two symmetric cracks (Fig. 3)

$$G=\frac{2H_1n_1\kappa_1^{n_1+1}}{(n_1+1)(n_1+2)}\Big[\Big(\frac{h_1}{2}-z_{1n_1}\Big)^{n_1+2}-\Big(-\frac{h_1}{2}-z_{1n_1}\Big)^{n_1+2}\Big] + 4h\frac{H_1}{n_1+1}\Big(\frac{F}{2bhH_1}\Big)^{(n_1+1)/n_1}-\frac{2F}{b}\Big(\frac{F}{2bhH_1}\Big)^{1/n_1}. \tag{38}$$

The fact that (38) is exact match of (28) verifies the J-integral non-linear solution (28).

2.2 Investigation of multilayered CLS beam

The J-integral solution in segment A of the multilayered CLS beam (Fig. 1) was found in the following way. The equations for equilibrium of lower crack arm cross-section were written as

$$N=\sum_{i=1}^{n_L}\int_{z_{1i}}^{z_{1i+1}}\sigma_i b dz_1\,, \tag{39}$$

$$M=\sum_{i=1}^{n_L}\int_{z_{1i}}^{z_{1i+1}}\sigma_i b z_1 dz_1\,, \tag{40}$$

where n_L is the layers number in the lower crack arm (Fig. 6). The coordinates z_{1i} and z_{1i+1} are defined in Fig. 6. By substituting of (2) and (9) in (39) and in (40), we obtained

$$N=b\sum_{i=1}^{n_L}\Big\{\frac{H_{1i}\kappa_1^{n_{1i}}}{n_{1i}+1}[(z_{1i+1}-z_{1n_1})^{n_{1i}+1}-(z_{1i}-z_{1n_1})^{n_{1i}+1}]\Big\}, \tag{41}$$

$$M=b\sum_{i=1}^{n_L}\Big\{\frac{H_{1i}\kappa_1^{n_{1i}}}{n_{1i}+2}[(z_{1i+1}-z_{1n_1})^{n_{1i}+2}-(z_{1i}-z_{1n_1})^{n_{1i}+2}] + \frac{H_{1i}\kappa_1^{n_{1i}}z_{1n_1}}{n_{1i}+1}[(z_{1i+1}-z_{1n_1})^{n_{1i}+1}-(z_{1i}-z_{1n_1})^{n_{1i}+1}]\Big\}, \tag{42}$$

where N and M are determined by (5) and (6), respectively.

It should be mentioned that at $n_L=1$ equations (41) and (42) transform in (12) and (13), respectively.

Equations (41) and (42) should be solved with respect to z_{1n_1} and κ_1 by using the MatLab computer program.

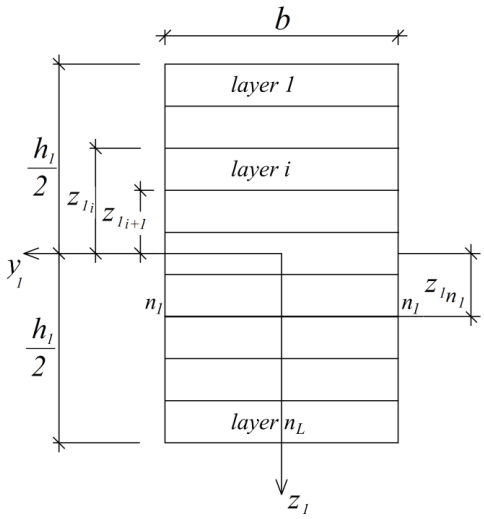

Fig. 6. Cross-section of the lower crack arm of CLS multilayered beam.

Formula (22) for the strain energy density was rewritten as

$$u_{0i} = \frac{H_{1i}[\kappa_1(z_1 - z_{1n_1})]^{n_{1i}+1}}{n_{1i}+1}, \quad i = 1, 2, \ldots, n_L. \tag{43}$$

The component of the J-integral were found as

$$p_{xi} = -\sigma_i = -H_{1i}\varepsilon^{n_{1i}}, \quad p_{yi} = 0, \quad ds = dz_1 \quad \text{and} \quad \cos\alpha = -1. \tag{44}$$

The J-integral in segment A of the multilayered CLS beam was written as

$$J_A = \sum_{i=1}^{n_L} \int_{z_{1i}}^{z_{1i+1}} \left[u_{0i}\cos\alpha - \left(p_{xi}\frac{\partial u}{\partial x} + p_{yi}\frac{\partial v}{\partial x}\right)\right] ds. \tag{45}$$

After substitution of (9), (19), (43) and (44) in (45), we derived

$$J_A = \sum_{i=1}^{n_L} \frac{H_{1i}n_{1i}}{(n_{1i}+1)(n_{1i}+2)} \kappa_1^{n_{1i}+1}[(z_{1i+1} - z_{1n_1})^{n_{1i}+2} - (z_{1i} - z_{1n_1})^{n_{1i}+2}]. \tag{46}$$

It should be specified that the un-cracked beam portion, $x > 0$, is loaded in eccentric tension, since the beam is multilayered with arbitrary arranged layers. Therefore, the curvature and the neutral axis coordinate in the un-cracked beam portion that are needed in order to find the J-integral solution in segment B of the integration contour (Fig. 1) were determined from the equilibrium equations (41) and (42).

For this purpose, (41) and (42) were modified in the following way: n_L, κ_1, z_{1i}, z_{1i+1} and z_{1n_1} were replaced with n, κ_3, z_{3i}, z_{3i+1} and z_{3n_3}, respectively. Besides, it was substituted $M = 0$ in (34). Then, the modified equations (33) and (34) should be solved with respect to κ_3 and z_{3n_3} by using the MatLab computer program.

Equation (43) was used to find the strain energy density. For this purpose, n_L, κ_1, z_1 and z_{1n_1} were replaced with n, κ_3, z_3 and z_{3n_3}, respectively.

The components of the J-integral were found as

$$p_{xi} = \sigma_i = H_{1i}\varepsilon^{n_{1i}}, \quad p_{yi} = 0, \quad ds = -dz_3 \quad \text{and} \quad \cos\alpha = 1. \tag{47}$$

The partial derivative was written as

$$\frac{\partial u}{\partial x} = \varepsilon = \kappa_3(z_3 - z_{3n_3}). \tag{48}$$

The J-integral in segment B was expressed as

$$J_B = \sum_{i=1}^{n} \int_{z_{3i+1}}^{z_{3i}} \left[u_{0i}\cos\alpha - \left(p_{xi}\frac{\partial u}{\partial x} + p_{yi}\frac{\partial v}{\partial x}\right)\right] ds\,. \tag{49}$$

After substitution of (47) and (48) in (49), we derived

$$)J_B = -\sum_{i=1}^{n} \frac{H_{1i}n_{1i}}{(n_{1i}+1)(n_{1i}+2)}\kappa_3^{n_{1i}+1}[(z_{3i+1} - z_{3n_3})^{n_{1i}+2} - (z_{3i} - z_{3n_3})^{n_{1i}+2}]. \tag{50}$$

Then (46) and (50) were substituted in (4) and the expression obtained was doubled in view of the symmetry

$$\begin{aligned} J = {} & 2\sum_{i=1}^{n_L} \frac{H_{1i}n_{1i}}{(n_{1i}+1)(n_{1i}+2)}\kappa_1^{n_{1i}+1}[(z_{1i+1} - z_{1n_1})^{n_{1i}+2} - (z_{1i} - z_{1n_1})^{n_{1i}+2}] \\ & - 2\sum_{i=1}^{n} \frac{H_{1i}n_{1i}}{(n_{1i}+1)(n_{1i}+2)}\kappa_3^{n_{1i}+1}[(z_{3i+1} - z_{3n_3})^{n_{1i}+2} - (z_{3i} - z_{3n_3})^{n_{1i}+2}]. \end{aligned} \tag{51}$$

It should be mentioned that at $n_L = 1$ and $n = 1$ equation (51) transforms in (28).

The non-linear solution (51) was verified by analyzing the strain energy release rate with the help of equation (32). For this purpose, the multilayered CLS beam complimentary strain energy was written as

$$U^* = \sum_{i=1}^{i=n_L} \int_{z_{1i}}^{z_{1i+1}} u_{0i}^* bad z_1 + \sum_{i=1}^{i=n} \int_{z_{3i}}^{z_{3i+1}} u_{0i}^* b(l-a) dz_3\,. \tag{52}$$

Equation (36) was rewritten as

$$u_{0i}^{*} = H_{1i}\frac{n_{1i}\varepsilon^{n_{1i}+1}}{n_{1i}+1}, \quad i = 1, 2, \ldots, n, \tag{53}$$

where the strain, ε, in the lower crack arm and in the un-cracked beam portion is found by (9) and (48), respectively. After substitution of (9), (48) and (53) in (52), we obtained

$$U^{*} = ba\sum_{i=1}^{n_L}\frac{H_{1i}n_{1i}}{(n_{1i}+1)(n_{1i}+2)}\kappa_1^{n_{1i}+1}[(z_{1i+1}-z_{1n_1})^{n_{1i}+2}-(z_{1i}-z_{1n_1})^{n_{1i}+2}] \tag{54}$$
$$+\, b(l-a)\sum_{i=1}^{n}\frac{H_{1i}n_{1i}}{(n_{1i}+1)(n_{1i}+2)}\kappa_3^{n_{1i}+1}[(z_{3i+1}-z_{3n_3})^{n_{1i}+2}-(z_{3i}-z_{3n_3})^{n_{1i}+2}].$$

The expression derived by substitution of (54) in (32) was doubled in view of the symmetry (Fig. 1)

$$G = 2\sum_{i=1}^{n_L}\frac{H_{1i}n_{1i}}{(n_{1i}+1)(n_{1i}+2)}\kappa_1^{n_{1i}+1}[(z_{1i+1}-z_{1n_1})^{n_{1i}+2}-(z_{1i}-z_{1n_1})^{n_{1i}+2}] \tag{55}$$
$$-\,2\sum_{i=1}^{n}\frac{H_{1i}n_{1i}}{(n_{1i}+1)(n_{1i}+2)}\kappa_3^{n_{1i}+1}[(z_{3i+1}-z_{3n_3})^{n_{1i}+2}-(z_{3i}-z_{3n_3})^{n_{1i}+2}].$$

Obviously, (55) is exact match of equation (51). This fact is a verification of the non-linear solution (51).

3 Effects of Material Properties and Crack Location on Fracture

Parametric analyses were carried-out of the non-linear fracture behaviour of multi-layered CLS beam. The aim of these analyses was to evaluate the effects of material properties and crack location along the beam height on the fracture. For this purpose, calculations were performed of the J-integral value by using equation (51) assuming that $F = 600$ N, $b = 0.02$ m and $h = 0.0015$ m. A tri-layered system was analyzed (Fig. 7). The thickness of each layer was $t_l = 0.001$ m. In order to evaluate the effect of crack location on the non-linear fracture behaviour, two beam configurations were considered (with a crack located between layers *2* and *3* (Fig. 7a) and with a crack between layers *1* and *2* (Fig. 7b)). The J-integral values generated by these calculations were presented in non-dimensional form by using the formula $J_N = J/(H_{11}b)$. The J-integral was plotted against H_{12}/H_{11} ratio (it was assumed that $H_{13}/H_{11} = 1.4$) in Fig. 8 for the two beam configurations shown in Fig. 7. It can be observed in Fig. 8

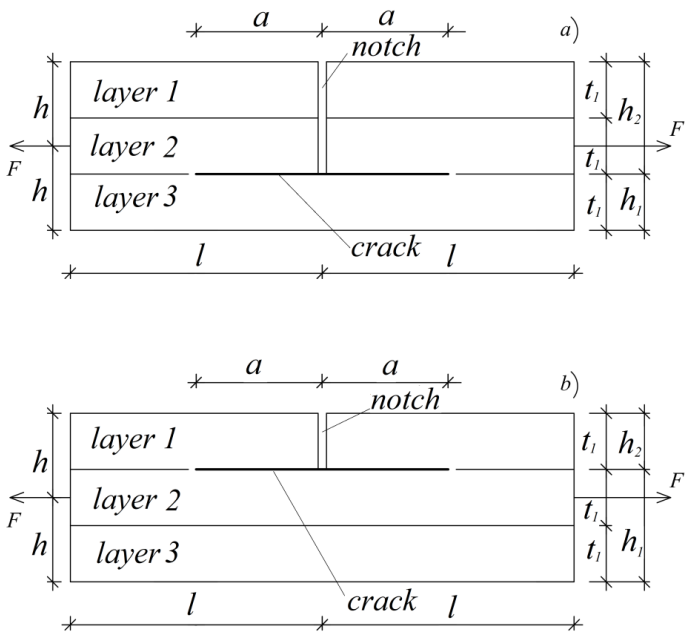

Fig. 7. Tri-layered CLS beam with crack located between: (a) layers *2* and *3*; and (b) layers *1* and *2*.

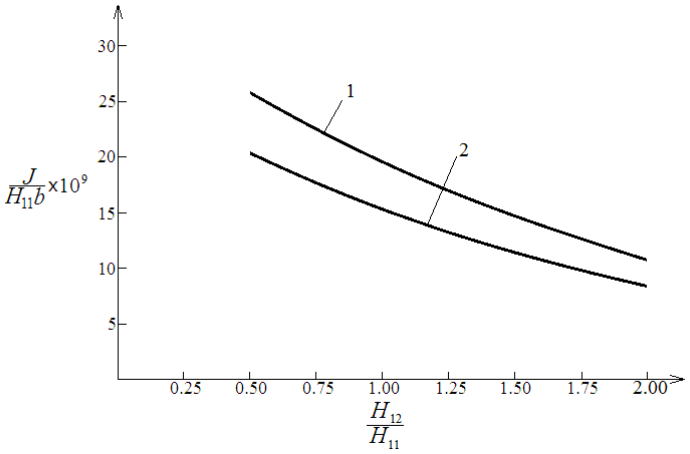

Fig. 8. The J-integral value in non-dimensional form plotted against H_{12}/H_{11} ratio (curve *1* – for crack location shown in Fig. 7a, curve *2* – for crack location shown in Fig. 7b).

that the J-integral value decreases with increasing H_{12}/H_{11} ratio. This finding was explained with the increase of CLS beam stiffness. Also, the curves in Fig. 8 indicate that the J-integral value decreases with changing the crack location from this shown in Fig. 7a to that in Fig. 7b (this finding was attributed to increase of the lower crack arm thickness and to decrease of the bending moment in the lower crack arm).

The variation of J-integral value in the beam configuration shown in Fig. 7a as a function of H_{13}/H_{11} ratio, assuming that $H_{12}/H_{11} = 1.2$, is illustrated in Fig. 9. One can observe that the increase of H_{13}/H_{11} ratio leads to decrease of the J-integral value. Finally, the influence of non-linear material behaviour on the fracture was analyzed. For this purpose, the J-integral value was calculated assuming linear-elastic material behaviour (the linear-elastic solution was derived by substitution of $n_{1i} = 1$ in equation (51)) and was plotted in non-dimensional form against H_{13}/H_{11} ratio in Fig. 9 for comparison with the non-linear solution. The curves in Fig. 9 indicate that the material non-linearity leads to increase of the J-integral value. Therefore, the material non-linearity has to be taken into account in fracture behaviour based safety design of multilayered beams.

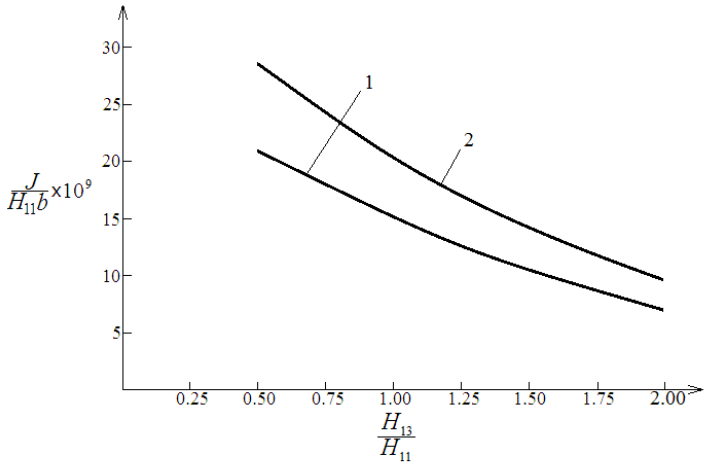

Fig. 9. The J-integral value in non-dimensional form plotted against H_{13}/H_{11} ratio (curve *1* – linear-elastic material behaviour, curve *2* – non-linear material behaviour).

4 Conclusions

Non-linear delamination fracture in the CLS multilayered configuration was analyzed by the classical beam theory. The mechanical response of beam layers was modelled by using a power-law stress-strain relation. Each layer may have different thickness. Also, the mechanical behaviour of each layer may be characterized by different val-

ues of material constants in the stress-strain relation. The delamination crack was located arbitrary along the beam height. Fracture in the homogeneous CLS beam was studied too. The fracture behaviour was investigated by using the J-integral approach. In order to verify the J–integral non-linear solutions derived, analyses of the strain energy release rate were developed with considering the material non-linearity. The influence of materials properties and crack location on the fracture was evaluated. The analysis revealed that the J-integral value decreases with increasing the lower crack arm thickness. It was found also that the material non-linearity leads to increase of the J-integral value (this finding indicates that the material non-linearity has to be considered in fracture behaviour based safety design of multilayered structures). The solutions obtained are very useful for parametric studies, since the simple formulae derived capture the essential of non-linear fracture in the CLS multilayered beam. The results can be used to optimize the multilayered beams with respect to their fracture performance. The present study contributes for the understanding of fracture in multilayered beams with non-linear material behaviour.

REFERENCES

[1] DAVIDSON, B. D., V. SUNDARARAMAN. A Single-Leg Bending Test for Interfacial Fracture Toughness Determination. *Int. J. Fract.*, **78** (1996), 193-210.

[2] NARIN, J. A. Energy Release Rate Analysis of Adhesive and Laminate Double Cantilever Beam Specimens Emphasizing the Effect of Residual Stresses. *Int. J. Adh. Adhes.*, **20** (1999), 59-70.

[3] YEUNG, D. T. S., D. C. C. LAM, M. M. F. YUEN. Specimen Design for Mixed Mode Interfacial Fracture Properties Measurement in Electronic Packages. *J. Electr. Packag.*, **122** (2000), 67-72.

[4] SZEKRENYES, A., W. M. VICENTE. Interlaminar Fracture Analysis in the GII-GIII Plane Using Prestressed Transparent Composite Beams. *Composites Part A: Appl. Sci. Manuf.*, **43** (2012), 95-103.

[5] SZEKRENYES, A. Fracture Analysis in the Modified Split-Cantilever Beam Using the Classical Theories of Strength of Materials. *J. Phys.: Conference Series*, **240** (2010), 012030.

[6] GUADETTE, F. G., A. E. GIANNAPOULOS, S. SURESH. Interfacial Cracks in Layered Materials Subjected to a Uniform Temperature Change. *Int. J. Fract.*, **28** (2001), 5620-5629.

[7] JIAO, J., G. K. GURUMURTHY, E. J. KRAMER, Y. SHA, C. Y. HUI, P. BORGESEN. Measurement of Interfacial Fracture Toughness Under Combined Mechanical and Thermal Stress. *J. Electron Packag.*, **120** (1998), 325-349.

[8] MARKOV, I., D. DINEV. Theoretical and Experimental Investigation of a Beam Strengthened by Bonded Composite Strip. *Reports of International Scientific Conference VSU'*2005, 2005.

[9] YOKOZEKI, T., T. OGASAWARA, T. AOKI. Correction Method for Evaluation of Interfacial Fracture Toughness of DCB, ENF and MMB Specimens with Residual Thermal Stresses. *Compos. Sci. Technol.*, **68** (2008), 760-767.

[10] HSUESH, C. H., W. H. TUAN, W. C. J. WEI. Analyses of Steady-State Interface Fracture of Elastic Multilayered Beams Under Four-Point Bending. *Scripta Mater.*, *60* (2009), 721-724.

[11] HER, S-C., W-B. SU. Interfacial Fracture Toughness of Multilayered Composite Structures. *Strength of Materials*, **47** (2015) No. 1; DOI:10.1007/s11223-015-9646-y.

[12] RICE, J. R. A Path Independent Integral and the Approximate Analysis of Strain Concentration by Notches and Cracks. *J. Appl. Mech.*, **35** (1968), 379-386.

[13] CHEREPANOV, G. Brittle Materials Fracture Mechanics. Nauka, M., 1974.

[14] BROEK, D. Elementary Engineering Fracture Mechanics. Springer, 1986.

[15] HOFF, N. J. The Analysis of Structures. John Wiley&Sons, New York, 1956.

[16] NADAI, A. Theory of Flow and Fracture of Solids, 2. McGraw-Hill, New York, 1963.

[17] SEELY, F. B., J. O. SMITH. Advanced Mechanics of Materials, John Wiley&Sons, New York, 1967.

[18] WASHIZU, K. Variational Methods in Elasticity and Plastici, Pergamon press, Oxford, 1974.

[19] HUTCHINSON, J. W., Z. SUO. Mixed Mode Cracking in Layered Materials. *Adv. Appl. Mech.*, **64** (1992), 804-810.